TECHNICAL NOTE

Development and application of a portable LIPS system for characterising copper alloy artefacts

J. Agresti · A. A. Mencaglia · S. Siano

Abstract We report the development of a novel portable and low-cost laser induced plasma spectroscopy (LIPS) system and describe the application method for quantitative characterisation of quaternary copper alloy artefacts. The device was carefully calibrated and phenomenologically characterised using a set of reference samples. The reliability of the quantitative measurement of the depth profile and bulk compositions was assessed through crossed comparisons with traditional analytical techniques. Finally, the LIPS system was applied to investigate a museum figurine of unknown origin composed of several pieces, which is representative of a typical authentication problem.

Introduction

As recognised since the early experimentations, laser induced plasma spectroscopy (LIPS) represents a very attractive approach in several fields of application [1–3]. It can provide significant advantages with respect to traditional elemental techniques whenever non-invasiveness, versatility, portability, real-time measurements, and low cost represent key factors for addressing the specific analytical problem under study. All these features are particularly important when investigating objects of art and historical interest, which has stimulated a

J. Agresti (✉) · A. A. Mencaglia · S. Siano
Istituto di Fisica Applicata "Nello Carrara"-CNR,
Via Madonna del Piano 10,
50019 Sesto Fiorentino (FI), Italy
e-mail: j.agresti@ifac.cnr.it

number of works dedicated to archaeometrical and conservation problems during the last decade [4].

Significant efforts were devoted to designing experimental LIPS set-ups and to optimising analytical protocols for characterising painted surfaces [5], ceramics [6], glasses [7], and Cu alloy artefacts [6, 8–13]. The latter application appears particularly interesting and promising since usually many analytical spots are needed to achieve representative elemental characterisations. Both small and large Cu alloy artworks are often assembled from independent pieces and include repair patches, plugs, core pins, and brazing materials of different compositions, whose measurement using traditional techniques [inductively coupled plasma (ICP) optical emission spectroscopy (OES), ICP mass spectrometry, atomic absorption spectroscopy (AAS)] would produce unacceptable damage. On the other hand, also a supposedly non-invasive technique such as portable X-ray fluorescence (XRF) has strong limitations in Cu alloy archaeometallurgy.

Reliable elemental quantification of ancient bronzes using XRF requires deep preliminary cleaning to remove encrustations and mineralisation layers, which can be much more destructive than LIPS and other techniques. Furthermore, in many cases surface abrasion was not sufficient to overcome the problems associated with enrichment and depletion phenomena, which characterise the corrosion of Cu alloys. Conversely, XRF is successfully used and well established in comparative statistical investigations (see, e.g., [14]).

In principle, LIPS can represent the best approach for achieving thorough non-invasive analyses of the surface corrosion layers and metal alloys underneath. However, for various reasons this powerful tool is still far from being used in the common archaeometallurgical and conservation practices, being mostly confined to use in scientific

laboratories. This is due to the difficulty in achieving reliable quantifications, as well as to the cost and complexity of the instrumentation usually employed, based on electro-optically Q-switched Nd:YAG or/and ultrashort lasers (single or double pulse) [13, 15], an echelle spectrometer, and an intensified CCD camera.

Although simplified devices based on compact Czerny-Turner spectrometers and CCD detectors were also proposed [16–18], and some of them are now available on the market, no proof of their effectiveness to address concrete archaeometallurgical problems was provided. There are various reasons for the limitations of these devices for quantitative analysis. In particular, the lack of repeatability can be associated with the use of passively Q-switched lasers, low intensity to the target, instability of the optical alignment, low signal-to-noise ratio, (SNR) and other factors. In fact, these systems are not used in archaeometallurgical studies, and only a few preliminary works based on cumbersome lasers and gated detectors are available [6, 8–13].

However, clear indications about the possibility of developing compact and low-cost single-pulse LIPS systems able to provide quantitative analysis of Cu alloys were reported in previous studies. These pointed out that the method of calibration curves, introduced since the early applications of the technique, represents the most reliable approach for quantification, which is more sensitive when using nanosecond rather than femtosecond lasers [13] and exhibits an improved reproducibility when the laser intensity is increased up to several tens of gigawatts per square centimetre [8]. In this way, the lack of plasma stoichiometry is expected to not affect the reliability of the quantification.

On the basis of these criteria and in view of in situ applications on small and large artworks, we designed, assembled, and calibrated a novel portable and low-cost LIPS system dedicated to the quantitative analysis of the binary, ternary and quaternary Cu alloys. Calibration curves of Sn, Zn, and Pb contents with regression coefficients above 99% were successfully obtained. The system was tested and validated through crossed measurements where LIBS results were compared with those provided by ICP-OES, AAS, and scanning electron microscopy-energy dispersive X-rays (SEM-EDX) on prepared laboratory samples and museum artefacts. Furthermore, the work also focuses on some methodological aspects concerning the calibration procedure, measurement of the elemental depth profiles, and extraction of the bulk composition from the latter. We outline the fundamental importance and usefulness of the measurement of the elemental depth profile using up to some thousands of laser pulses; this was usually neglected in previous studies. The work aims at providing the first concrete demonstration that an optimised, low-cost, and portable LIPS device along with a suitable application method can fully address the typical elemental character-isation problems of Cu alloy objects of art and historical interest.

Instrumentation

The LIPS system was devised to maximise the cost-benefit ratio. We assumed as the main constraints of the cost reduction the achievement of reliable quantitative measurement of quaternary Cu alloy and easy portability. These conditions led us to select a compact Q-switched Nd:YAG laser (1,064 nm, 7-ns pulse duration, 0–20-Hz pulse repetition rate) as the excitation source. The length of the laser head is 17 cm and the total weight (head and power supply) is about 14 kg, which allowed us to restrict the total weight of the LIPS device to around 20 kg (laser, optics, spectrometer, PC, and case).

The laser emits an almost top-hat, low-divergence beam (0.8 mrad, using a graded reflectivity mirror), with a spot diameter of 2.5 mm and a maximum energy of 50 mJ/pulse (Ultra 50 CFR, BigSky). Such a laser source allows a sufficiently high intensity to be achieved using common planoconvex lenses. Here, it is about 100 GW/cm^2 using a focusing length of 60 mm.

The focus is set 1 mm beneath the irradiated surface to avoid the total shielding of the target surface due to the occurrence of air breakdown and to improve the reproducibility of the plasma emission [19]. Under this condition, the laser spot on the sample has a diameter of about 120 μm and a corresponding maximum intensity of about 63 GW/cm^2.

Plasma emission is collected with an off-axis parabolic mirror (M_1) at an angle of 60° with respect to the target surface (Fig. 1). This angle was preferred with respect to 45° and 30°, also widely available on the market, to reduce the lateral size of the tip of the instrument, which allows access to relatively deeper undercuts on the object under study.

The light collected by M_1 is coupled in a bundle of four optical fibres (200-μm core diameter) via a second parabolic mirror (M_2). The fibres are connected to the entrance slits (10 μm) of four compact Czerny-Turner spectrometers (2,400 grooves/mm) equipped with CCD linear array detectors (AvaSpec-2048 FT, Avantes), which cover the spectral range between 200 and 630 nm with a resolution of 0.06 nm.

The reflective imaging set-up was preferred with respect to those typically used (fibre or lens-fibre collection) for various reasons. It is not affected by spherical and chromatic aberration, thus allowing the simultaneous illumination of the four spectrometers with sufficient levels of signal. The relatively high numerical aperture (NA) of the collecting mirror (M_1; NA=0.37), and the matching of the NA of the focusing one (M_2) with the numerical
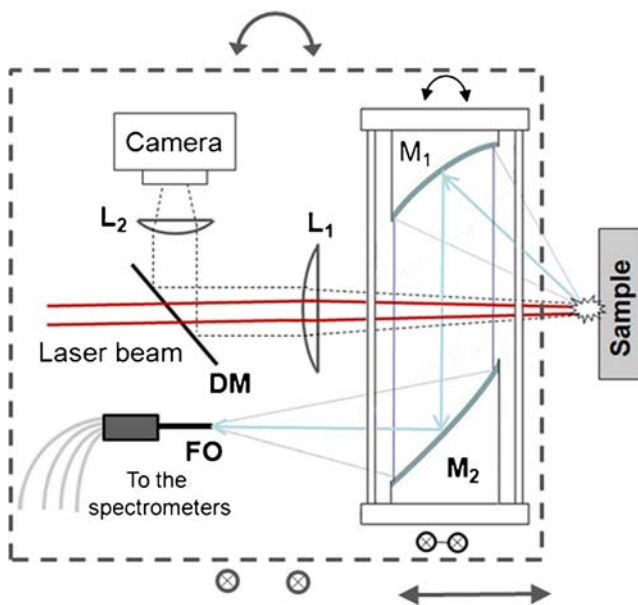
Fig. 1 The optical set-up of the laser induced plasma spectroscopy (LIPS) head (arbitrary sizes). *Arrows* indicate rotation and translation stages, which allow the alignment. *DM* dichroic mirror, *FO* bundle of four optical fibres

aperture of the optical fibres (NA=0.22) improve the efficiency of the optical set-up. It was selected after testing several alternative solutions.

Preliminary measurements aimed at assessing the conditions for the best shot-to-shot repeatability on the homogeneous reference samples led us to set the focal point of the collecting mirror (M_1) about 1 mm from the irradiated surface.

The optical set-up was preliminarily aligned using a flat bronze sample orthogonal to the laser beam and the signal was maximised by suitably orienting the coupled mirrors (Fig. 1). In operative conditions, the focal position and orthogonal orientation of the LIPS head are achieved by means of rotation and translation stages. This set-up and its alignment is of crucial importance to achieve sufficiently high illumination of the non-intensified CCD arrays in all the operative conditions.

As usual, the acquisition by the CCD detectors is delayed with respect to the laser pulse to cut off the early continuum spectrum generated by inverse bremsstrahlung. The detectors allow for a precise setting of time delays of more than 1.3 µs (reset time) with respect to an external trigger (42-ns minimum variation step). The timing of the whole system is driven using a pulse and delay generator, which triggers the acquisition 500 ns after the laser pulse [20]. In this configuration the SNR and the signal-to-background ratio are relatively high, whereas higher delays reduce the SNR, thus affecting the detection of low-concentration and trace elements. At the same time, higher delays act against a further simplification of the LIPS

devices devoted to the chemical analysis of Cu alloys through the use of passively Q-switched Nd:YAG lasers, optical triggering, and by setting the delay of the spectrometer to the minimum one (1.3 µs).

Calibration curves

The LIPS system was calibrated using a set of homogenised reference samples (annealed at 700 °C for 2 h) to achieve the quantitative measurements of the main elements of binary, ternary, and quaternary Cu alloys. The samples include home-made castings cast using pure elements, such as, in particular, electrolytic Cu, along with some certified standards. In all cases the composition was verified using SEM-EDX, AAS, or ICP-OES.

The internal standard approach was applied in calibration measurements, i.e. using the integrated line intensity of the analyte normalised to the Cu line intensity. As known, this is the way to compensate absolute intensity fluctuations associated with shot-to-shot variations of the ablation rate [21] and excitation parameters, as well as with possible self-absorption phenomena.

Spectral lines suitable for quantifying the elements of interest (Cu, Sn, Zn, Pb) were preliminarily selected among those which do not exhibit relevant overlapping and whose associated calibration curves are not affected by matrix effects. As shown in Table 1, the lines selected for both the analytes and the internal standard have very similar excitation energies, which corresponds to some extent to comparable excitation effects. For Sn and Pb it was possible to select lines very close to those of Cu (same detector array, within about 15 nm), whereas the best line for Zn (472.22 nm) was rather far away, in the range of the adjacent CCD array (third), which led us to select for this element a closer Cu reference line (458.7 nm). Finally, we also selected a Cl line for semiquantitative analyses of this element, which are of interest as an indicator of natural corrosion, as well as in view of applications of LIPS for diagnostic and monitoring purposes.

Line intensity ratios of Sn, Zn, and Pb were measured as a function of the corresponding weight fractions between 0 and 15 wt%, 0 and 35 wt%, and 0 and 13 wt%, respectively. The experimental plots along with linear fits are displayed in Fig. 2. The choice of the Sn and Zn concentration domains was determined by the extension of the α(Cu) phases of binary bronzes and brasses, respectively, whereas the Pb content was limited since above 10–15 wt% this element starts to produce significant intergranular segregations, which are of sizes comparable to the size of the laser spot, with a consequent increase of line intensity fluctuations. At higher Sn and Zn contents, the precipitation of the eutectoid δ(Cu) phase produces a relevant change of the metal matrices with

Table 1 Spectral lines selected for quantitative analyses of Sn, Zn, and Pb, and semiquantitative analysis of Cl

Line (nm)	E_k (eV)	E_i (eV)
Cu I (296.12)	5.57	1.39
Sn I (284)	4.79	0.42
Pb I (283.3)	4.37	0
Zn I (472.22)	6.65	4.02
Cu I (458.7)	7.8	5.10
Cl I (422.64)	11.85	8.92

a consequent change of the slopes of the calibration curves and an increase of fluctuations owing to the growing of non-homogeneity.

Each point in the calibration plots was obtained according to the following procedure. The samples were polished and preliminarily irradiated with some shots (one to five) to remove any possible deposits and oxidation residues, as well as to stabilise the surface roughness and reflectivity, which can significantly affect the laser energy coupling to the target. Afterwards, the normalised line integral of the analyte was measured over about 1,000 shots to verify its stability while the ablation depth increases, which is to say to check the homogeneity of the plasma region measured during the hole drilling. Figure 2d provides evidence of the repeatability of the Sn and Pb intensity ratios for a ternary alloy sample.

Such good reproducibility was assessed for most of the reference samples, apart from some rare cases where drift of the data slightly outside a typical fluctuation was observed, which is likely attributable to non-homogeneity of the specific sample. However, the intensity ratios plotted in Fig. 2 were obtained by averaging over at least 200 and up to 1,000 laser shots. The typical error bars (standard deviations) are lower than 10% and the correlation coefficients of the linear fits are above 99%.

Some cross-check measurements are superimposed on the calibration plots (circles in Fig. 2), where the measured LIPS intensity ratios are associated with the actual compositions as measured using AAS, SEM-EDX, and ICP-OES. The latter were correctly measured by LIPS with an accuracy better than 10% in most cases (Table 2). Similar assessments accompany our applications of the instrument in concrete archaeometallurgical and conservation problems whenever a minimally non-invasive material sampling is possible on the artefact under study.

The error bars of the calibration curves in Fig. 2a–c and the example in Fig. 2d provide evidence of the good repeatability achieved on reference samples of intensity ratios, which remain relatively stable (within the accuracy mentioned) over some thousands of laser shots.

To better describe the experimental conditions, let us note that the lack of a time gating, which is essential for assuming the hypothesis of local thermodynamic equilibrium, is here

Fig. 2 Sn (**a**), Zn (**b**), and Pb (**c**) calibration curves as achieved by fitting line intensity ratios of a set of reference samples (*squares*) and an example of signal stability (**d**) for a ternary Cu alloy sample. *Circles* represent test measurements on samples measured with other techniques and further standards (Table 2)
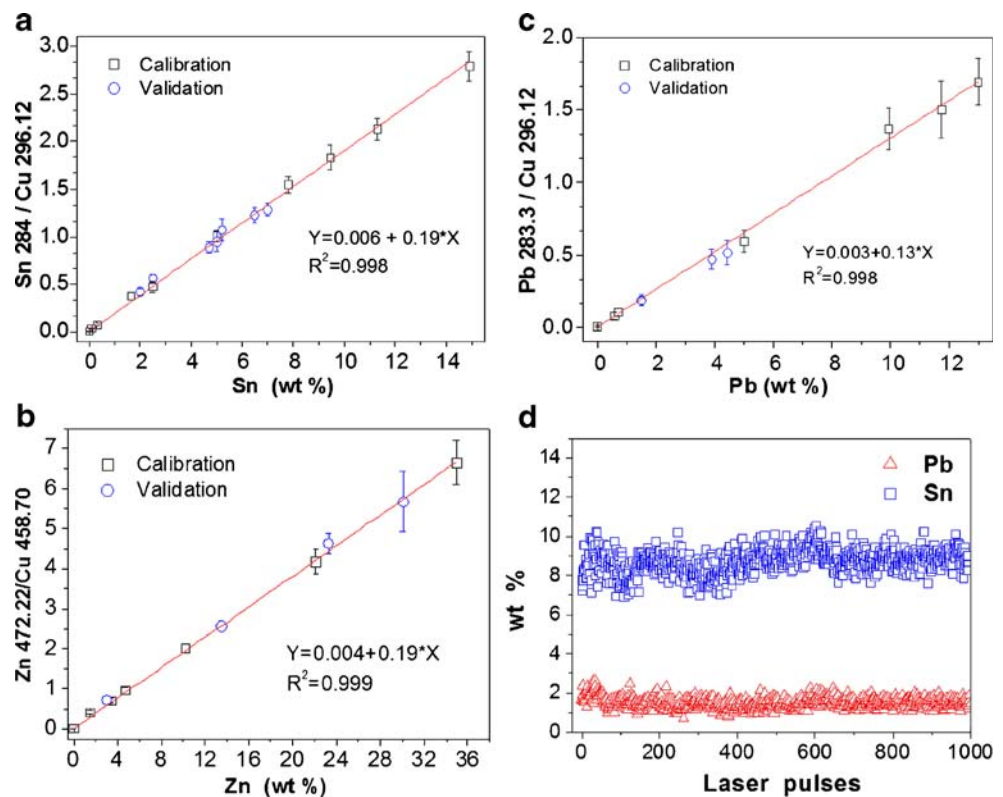
Table 2 Comparison between elemental contents (wt%) of samples measured by different techniques and commercial standards (nominal) and the corresponding laser induced plasma spectroscopy (*LIPS*) results

Sn	Pb	Zn	Sn LIPS	Pb LIPS	Zn LIPS
6.48/AAS			6.4±0.4		
7.04/AAS			6.7±0.3		
4.71/ICP			4.6±0.3		
2.1±0.1/EDX	1.5±0.1/EDX	13.5±0.4/EDX	2.2±0.2	1.5±0.3	13.5±0.7
2.5±0.2/EDX	1.5±0.1/EDX	3.0±0.2/EDX	2.9±0.2	1.4±0.2	3.6±0.4
5.2±0.3/EDX			5.6±0.6		
5.11±0.3/ICP			5.0±0.6		
	3.89/AAS			3.6±0.5	
		23.3/nominal			24.4±1.4
		30.1/nominal			29.8±3.9
	4.4/nominal			4.0±0.6	

AAS atomic absorption spectroscopy, *ICP* inductively coupled plasma, *EDX* energy-dispersive X-rays

practically compensated by the intrinsic temporal cut-off of the system. As shown in Fig. 3, the lifetime of the spectral lines of interest, as they are seen by the spectrometer, is around 3 μs, which corresponds to an effective integration time of 2.5 μs, which is similar to those typically used with gated systems. Thus, it is likely that no relevant undesired instability effects beyond the local thermodynamic equilibrium domain are registered by the CCD detector during the long integration time (2 ms). This certainly contributes to the reproducibility and reliability of the quantification found in the experiment.

The detection limits of Sn, Pb, and Zn (the concentration that produces a signal 3 times larger than the standard deviation of the noise, σ) can be calculated by converting the ratio between 3σ (background-subtracted signal) and the Cu line intensities of almost pure Cu in terms of weight percentage content using the corresponding calibration curves. If an RMS noise amplitude of 20 counts and the minimum integration window corresponding to the resolution of the spectrometer are assumed, the calculated detection limits are 0.09, 0.14, and 0.06% for Sn, Pb, and Zn, respectively. They are mostly determined by the present technological choices (single-pulse laser, non-intensified CCD detector) but also to some extent by the selection of the spectral lines used for the analysis. Other Cu, Sn, Pb, and Zn lines can be employed for trace analysis and give lower detection limits in the low-concentration range. However, considering the degree of reliability for the wide range of concentrations covered by the calibration curves, the quantification limits do not represent a problem for most of the technological problems encountered in the study of bronze and brass artefacts of art or historical interest.

The calibration curves obtained were implemented in a home-written code, which synchronises the laser emission and spectrometer acquisitions and then provides real-time elemental depth profiles.

Fig. 3 Time evolution of integrated line intensities (**a**) and of a spectral window of interest (**b**)

Depth profiles

Elemental depth profiles can represent a powerful investigation approach to different knowledge and conservation problems, which justifies some specific insights.

Depth profiles of polished homogeneous bronze samples were investigated to estimate the average ablation rates and the response of the system during a depth profile measurement. The ablation depths were measured as a
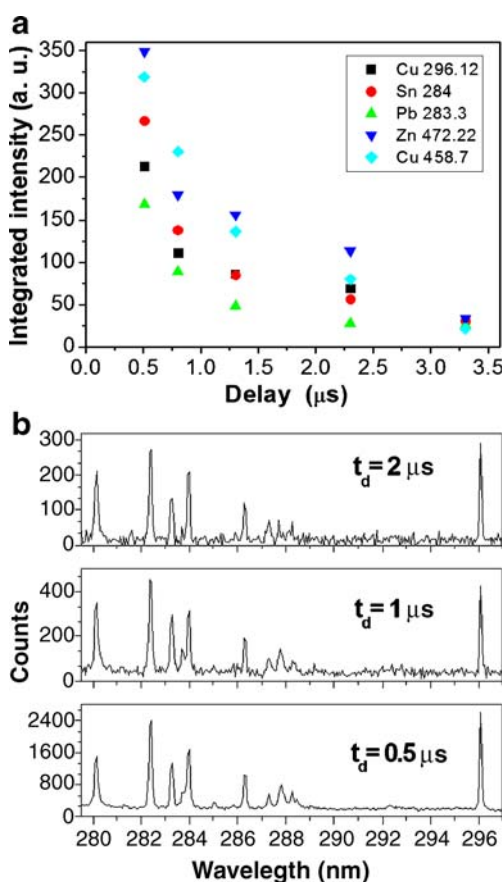
function of the number of pulses using an optical microscope equipped with a calibrated micrometric focusing stage. It was found that the average ablation rate depends on the composition of the sample and varies as a function of depth. Figure 4 shows the ablation depth measured for two samples, which represent to some extent extreme conditions of practical interest: a homogeneous quaternary Cu alloy (Cu 85 wt%, Sn 5 wt%, Pb 5 wt%, Zn 5 wt%) and a thick layer of cuprite (Cu_2O) of a Roman bronze coin. Despite the very different ablation rates, both curves exhibit a similar saturating behaviour, which is likely determined mostly by geometrical shielding of the laser beam while the depth of the hole increases. It is worth noting that the saturation is not necessarily associated with a marked conic shape of the hole, which is also strongly determined by the laser beam profile at the focus. The present beam profile (large top-hat central area surrounded by a peripheral ring with a slightly higher intensity) allows the production of rather high aspect ratio holes with relatively small diameter reductions over depths of some hundred microns.

In real conditions including surface and/or deep corrosion phenomena, we can just refer to the order of magnitude of the ablation depth since the ablation rate (i.e. spatial resolution of the LIPS analyses) likely varies between and around those associated with the two curves in Fig. 4, which are useful for rough estimations. Of course, in operative conditions, the final measurement of the total depth by a microscope could significantly help to refine the specific spatial scale of the elemental profile.

Furthermore, the compositional and microstructural distributions (metal and mineral phases) of real samples also affect the accuracy of the quantifications achieved by the present calibration curves (Fig. 2). This holds especially when ablating surface corrosion layers where the only intrinsic check is represented by the smoothness of the connection between the patina and bulk peak ratio data. The measurements show that for homogeneous samples geomet-

rical shielding, changes of the ablation rate, and plume shift during hole drilling do not relevantly affect quantitative depth profiles, which are repeatable and reliable, as also verified in practical cases of interest.

Example application

Following the general approach introduced above, the portable LIPS apparatus was applied to characterise a grotesque figurine (Fig. 5) from Florence's National Museum of Archaeology (inventory no. 2332, height 23 cm, first quoted in the Uffizi Gallery's inventories in 1784). The statuette is assembled from several pieces. At least the arms and feet are independent castings soldered to the body by soft brazing.

Quantitative analyses of the main elements of the Cu alloys were derived through the examination of the depth profiles of some thousands of laser shots. The quantitative compositional information is extracted from the average of the last hundred measurements, which exhibit almost constant line intensity ratios and provide direct evidence that the ablation has reached the metal bulk.

Two representative Sn and Cl depth profiles collected on the right arm (S9) and hood (S2), respectively, are displayed in Fig. 6. The Sn content of the former shows
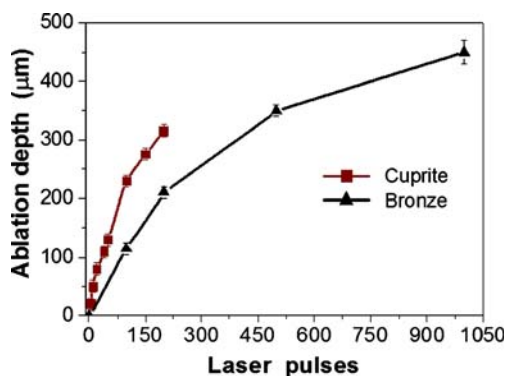

Fig. 4 Ablation depth as a function of the number of laser pulses for a quaternary bronze (85/5/5/5) and a natural cuprite layer of a Roman coin. The depth was measured using a z-calibrated microscope
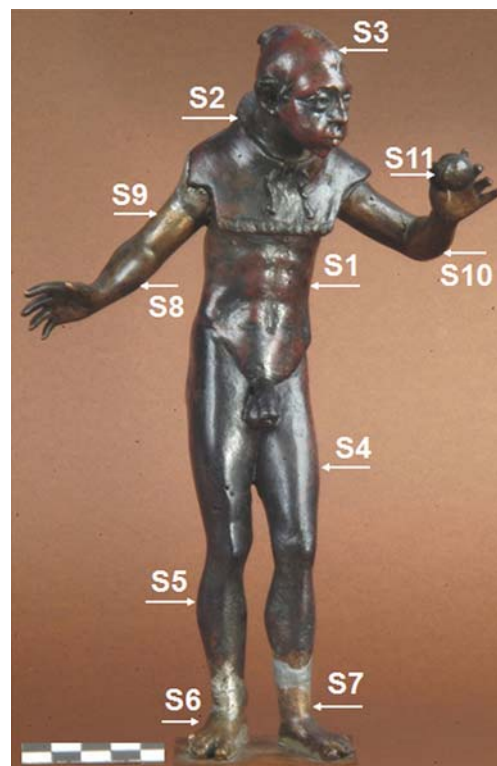

Fig. 5 Grotesque figurine from Florence's National Museum of Archaeology with indication of the sites analysed using LIPS

an initial modulation around the bulk values, then it becomes almost constant after about 120 shots, whereas the initial high value of the Cl line rapidly approaches zero after about 20 shots (Fig. 6a). These behaviours are slightly different with respect to the reference samples because of the initial modulation and the not negligible presence of Cl beneath the surface (20 shots correspond to about 20 μm). Such features are strongly "amplified" in the distributions measured on the hood (Fig. 6b). A significant Sn surface depletion, followed by local enrichment of a factor around 1.7 with respect to the bulk composition (rough estimation, see above), is achieved (constant composition) only after about 800 laser shots. Similarly, the decay of the structured Cl peak occurs after about the same number of shots. The fitting of the ablation depths measured on cuprite (Fig. 4) allows estimation of the bulk composition measured about 500 μm beneath the surface.

These behaviours shown in Fig. 6 are due to deep corrosion of the metal, as also independently assessed using time of flight neutron diffraction carried out at the pulsed neutron spallation source ISIS, Rutherford Appleton Laboratory, UK. The Rietveld refinements allowed calculation of weight fractions of cuprite (Cu_2O) and tenorite (CuO) up to 4 and 1 wt% in the bust of the figurine.

We believe such strong differences between the compositional distributions can be exploited to discriminate among different degrees of natural aging of Cu alloy artefacts and modern counterfeits. This topic will be dis-

cussed in some details in a forthcoming paper. Here, we simply add that the different compositions of the arms and feet with respect to the rest of the body corroborate the former are modern integrations on a genuine archaeological finding. As reported in Table 3, the arms and feet were crafted using a quaternary alloy, which is typical of a Renaissance art foundry rather than a Roman one, whereas the part recognised as genuine has a ternary composition compatible with ancient productions. The relatively large uncertainties of the parts integrated (Table 3) are likely due to their non-homogeneous compositions, as evident in the corresponding depth profiles.

Conclusions

Calibration curves, comparisons with traditional elemental techniques, and depth profiles on reference samples and museum artefacts show the compact and low-cost LIPS device developed in the present work is a reliable tool for characterising quaternary Cu alloy artefacts. This result was achieved by suitably selecting the laser system, designing an efficient and stable optical collector, and carefully calibrating the instrument using thoroughly verified reference samples.

Furthermore, we outlined the meaning, importance, and exploitation of elemental depth profiles extended up to thousands of pulses in the study of ancient Cu alloy objects. Bulk compositions should always be determined through the examination of depth profiles of the metal components as well as of the elements involved in the corrosion processes, such as, in particular, Cl.

In conclusion, the instrument and the methodological approach proposed are effective to solve a variety of archaeometallurgical problems related to alloy compositions and mineralisation phenomena of bronzes and brasses. We are
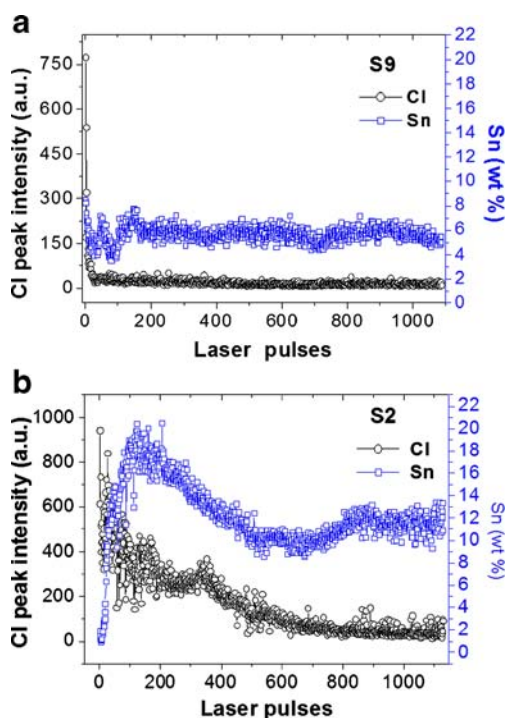

Fig. 6 Sn and Cl elemental depth profiles of the Cu alloy statuette investigated using LIPS (Fig. 5)

Table 3 Elemental contents in different zones of the Cu alloy statuette shown in Fig. 5

Site	Sn (%)	Pb (%)	Zn (%)
S1 (waist)	10.9±0.7	17.2±1.5	–
S2 (hood)	11.1±1.0	16.8±1.4	–
S3 (head)	10.4±0.7	8.7±0.5	–
S4 (left thigh)	13.7±0.7	10.7±0.5	–
S5 (right leg)	11.0±0.9	11.6±1.3	–
S6 (right foot)	5.3±0.3	5.5±0.7	3.6±0.4
S7 (left foot)	5.2±0.4	4.9±0.9	3.3±0.4
S8 (right arm)	6.7±1.1	4.2±1	5.3±1
S9 (right arm)	5.6±0.5	3.8±0.8	5.2±0.5
S10 (left arm)	5.2±0.5	3.9±1.4	4.9±0.9
S11 (fruit in left arm)	5.3±0.5	5±1.4	6.5±0.8

applying the device and the analytical protocol for the investigation of the authenticity of a number of statuettes from Florence's National Museum of Archaeology, as well as within archaeometallurgical studies aimed at the interpretation of the execution techniques applied in the production of unique Etruscan and Renaissance masterpieces.

Further efforts will be devoted to improve the analytical performances and to obtain further methodological insights. At the same time, a massive effort is going on, which is bringing the LIPS analysis into archaeometallurgical practice.

References

1. Radziemski LJ, Solarz RW, Paisner J (eds) (1989) Laser spectroscopy and its applications. Dekker, New York
2. Miziolek AW, Palleschi V, Schecter I (eds) (2006) Laser induced breakdown spectroscopy (LIBS): fundamentals and applications. Cambridge University Press, Cambridge
3. Cremers DA, Radziemski LJ (2006) Handbook of laser-induced breakdown spectroscopy. Wiley, New York
4. Giakoumaki A, Melessanaki K, Anglos D (2007) Anal Bioanal Chem 387:749–760
5. Anglos D, Couris S, Fotakis C (1997) Appl Spectrosc 51:1025–1030
6. Colao F, Fantoni R, Lazic V, Spizzichino V (2002) Spectrochim Acta Part B 57:1219–1234
7. Müller K, Stege H (2003) Archaeometry 45:421–433
8. Fornarini L, Colao F, Fantoni R, Lazic V, Spizzichino V (2005) Spectrochim Acta Part B 60:1186–1201
9. Fortes FJ, Cortes M, Simon MD, Cabalin LM, Laserna JJ (2005) Anal Chim Acta 554:136–143
10. Corsi M, Cristoforetti G, Giuffrida M, Hidalgo M, Legnaioli S, Masotti L, Palleschi V, Salvetti A, Tognoni E, Vallebona C, Zanini A (2005) Microchim Acta 152:105–111
11. De Giacomo A, Dell'Aglio M, De Pascale O, Gaudiuso R, Santagata A, Teghil R (2008) Spectrochim Acta Part B 63:585–590
12. Ferretti M, Cristoforetti G, Legnaioli S, Palleschi V, Salvetti A, Tognoni E, Console E, Palaia P (2007) Spectrochim Acta Part B 62:1512–1518
13. Elhassan A, Giakoumaki A, Anglos D, Ingo GM, Robbiola L, Harith MA (2008) Spectrochim Acta Part B 63:504–511
14. Ferretti M, Siano S (2007) Appl Phys A 90:97–100
15. De Giacomo A, Dell'Aglio M, Bruno D, Gaudiuso R, De Pascale O (2008) Spectrochim Acta Part B 63:805–816
16. Mueller M, Gornushkin B, Florek S, Mory D, Panne U (2007) Anal Chem 79(12):4419–4426
17. Cuñat J, Fortes FJ, Cabalín LM, Carrasco F, Simón MD, Laserna JJ (2008) Appl Spectrosc 62:1250–1255
18. Goujon J, Giakomaki A, Piñon V, Musset O, Anglos D, Georgiu E, Boquillon JP (2008) Spectrochim Acta Part B 63:1091–1096
19. Multari RA, Foster LE, Cremers DA, Ferris MJ (1996) Appl Spectrosc 50:1483–1499
20. Carranza JE, Gibb E, Smith BW, Hahn DW, Winefordner JD (2003) Appl Opt 42:6016–6021
21. St-Onge L, Sabsabi M, Cielo P (1997) J Anal At Spectrom 12:997–1004